Journal of ELECTRONIC MATERIALS, Vol. 42, No. 7, 2013
DOI: 10.1007/s11664-012-2249-5

Effects of Microstructural Evolution on the Thermoelectric Properties of Spark-Plasma-Sintered $Ti_{0.3}Zr_{0.35}Hf_{0.35}NiSn$ Half-Heusler Compound

O. APPEL,[1,4] M. SCHWALL,[2] D. MOGILYANSKY,[1] M. KÖHNE,[3] B. BALKE,[2] and Y. GELBSTEIN[1]

1.—Department of Materials Engineering, Ben-Gurion University of the Negev, Beer-Sheva, Israel. 2.—Institute of Inorganic and Analytical Chemistry, Johannes Gutenberg-University, Mainz, Germany. 3.—Robert Bosch GmbH, 70049 Stuttgart, Germany. 4.—e-mail: oshratba@post.bgu.ac.il

The MNiSn (M = Ti, Zr, Hf) half-Heusler semiconducting compounds are widely investigated due to their good potential for thermoelectric (TE) power generation applications. In the current work, the evolution of the transport and structural properties of the $Ti_{0.3}Zr_{0.35}Hf_{0.35}NiSn$ compound upon various thermal treatments was studied. The nominal composition was arc melted, ball milled, and spark plasma sintered (SPS). Following SPS, large Hf-rich domains were found by scanning electron microscopy (SEM) and energy-dispersive x-ray spectroscopy (EDS). Subsequently, the samples were subjected to homogenization treatments at 1163 K for 480 h and 610 h under argon atmosphere. Following these thermal treatments, the relative amount of the Hf-rich domains was reduced and they became smaller in size, with increasing thermal treatment duration. Nevertheless, no uniphased structure was reached. The dissolution of the Hf-rich domains in the half-Heusler matrix resulted in increase of both the Seebeck coefficient and electrical resistivity values and a decrease of the carrier concentration, attributed to elimination of these metallic domains. Resulting from the high atomic disorder caused by substitution at the M site, low thermal conductivity values of $\sim$3.8 W m^{-1} K^{-1} were obtained leading to high ZT values of up to 0.82 following SPS.

Key words: Half-Heusler, thermoelectrics, microstructure, efficiency figure of merit

INTRODUCTION

In recent years, interest in highly efficient thermoelectric (TE) materials has been continuously growing, due to the worldwide requirements to reduce greenhouse-gas emissions and global warming. Thermoelectric converters (TEC) are capable of direct conversion of residual heat generated by combustion engines, for instance, into electricity without the involvement of any moving parts. Thus, they not only decrease the reliance on fossil fuels but also actively reduce global warming effects.[1] TEC performance directly depends on the temperature gradient along the device, through the Carnot efficiency, and the intrinsic material properties, through the TE figure of merit (ZT), given by $ZT = \alpha^2 T/\kappa\rho$, where α is the Seebeck coefficient, ρ is the electrical resistivity, κ is the thermal conductivity, and T is the absolute temperature. TEC with high conversion efficiencies should possess high Seebeck coefficient, low electrical resistivity, and low thermal conductivity values and should operate over a broad temperature range.[2]

Current, state-of-the-art converters mainly contain tellurium-based TE compounds (e.g., PbTe and GeTe), which are too inefficient to be economic, due to both low efficiency values (5% to 10%) and expensive

(Received July 6, 2012; accepted August 28, 2012; published online September 29, 2012)

primary components.[3] Two additional drawbacks associated with these materials are their low operating temperatures (<773 K) and their environmentally unfriendly constituents (Pb). Against this background, half-Heusler (HH) compounds offer a very promising alternative for high-temperature applications up to 1000 K with adequate TE properties, combined with additional advantages such as environmental friendliness, low production costs, and future availability of raw materials.

The HH semiconducting compounds with 18 valence electrons are based on the general formula MYZ (M, Y = transition metals, Z = main group element). The compounds crystallize in the cubic MgAgAs-type structure ($F\bar{4}3m$) that is based on four interpenetrating face-centered cubic sublattices. The crystallographic sites (0, 0, 0) and (1/4, 1/4, 1/4) are occupied by two different transition-metal elements, the (1/2, 1/2, 1/2) sites are occupied by main group elements such as Sn and Sb, whereas the (3/4, 3/4, 3/4) site remains unoccupied.[1,4] Each occupied sublattice can be doped or substituted individually to enhance the TE efficiency.[4–6]

The main characteristics that make HHs so attractive for TE applications are their high Seebeck coefficient ($\sim$300 $\mu V\ K^{-1}$ at room temperature) and electrical conductivity ($\sim$1000 $\Omega^{-1}\ cm^{-1}$ to 10,000 $\Omega^{-1}\ cm^{-1}$) values. However, their thermal conductivity values tend to be quite high ($\sim$10 $W\ m^{-1}\ K^{-1}$), which can decrease their *ZT* values.[6]

Of all of the HH *n*-type compositions, the most investigated system, showing the highest TE potential, is MNiSn (M = Ti, Zr, Hf). In this system, the most common approach for reduction of the thermal conductivity is based on phonon scattering induced by mass and size differences resulting from isoelectronic substitutions at the M and/or Y positions of the compounds.[7–9] Another approach for *ZT* enhancement is based on electronic doping at the Z position by elements from group V (i.e., Sb, exhibiting a maximal *ZT* of 0.81 for the composition $Hf_{0.75}Zr_{0.25}NiSn_{0.975}Sb_{0.025}$[10]).

Although very high *ZT* values of up to $\sim$1.3[11] were reported for such isoelectronic substituted $Ti_xZr_yHf_{1-x-y}NiSn$ compounds, inconsistency of the reported values for very similar Ti, Zr, and Hf relative substitution amounts is still apparent, as shown in Fig. 1.

It can be seen from this figure that, although the Zr/Hf-substituted compound (curve b) exhibits higher *ZT* values compared with the nonsubstituted TiNiSn compound (curve a), not all of the multiple-substituted $Ti_xZr_yHf_{1-x-y}NiSn$ compounds exhibit higher *ZT* values than the latter. It can be seen that two very similar compositions of $\sim Ti_{0.3}Zr_{0.35}Hf_{0.35}NiSn$ (curves g and e), with a slight variation of the Zr/Hf ratio, exhibit lower *ZT* values than those of $Zr_{0.5}Hf_{0.5}NiSn$ (curve b), at least at several of the investigated temperatures. A third, very similar composition of $Ti_{0.37}Zr_{0.37}Hf_{0.26}NiSn$ (curve f) exhibits much higher *ZT* values of up to 1. Taking into account that all three of these similar compositions were processed and thermally treated

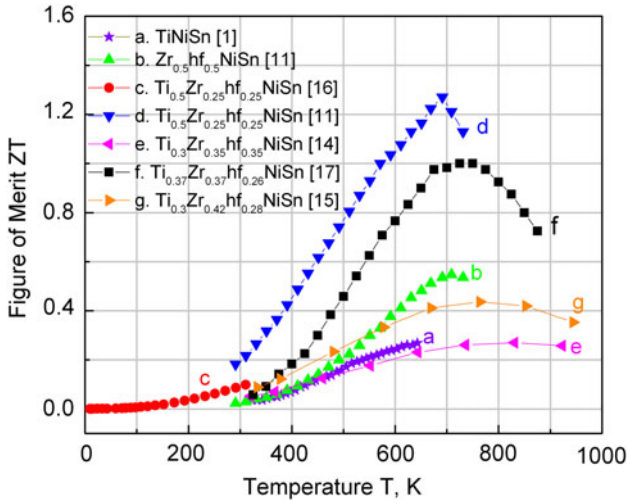

Fig. 1. Recently reported *ZT* values of selected $Ti_xZr_yHf_{1-x-y}NiSn$ compounds.[1,11,14–17]

under different conditions, it is obvious that atomic ordering and microstructural effects have a major influence on the resulting TE properties. A similar discrepancy is apparent on comparing two other HH curves of $Ti_{0.5}Zr_{0.25}Hf_{0.25}NiSn$ (curves c and d), processed by different powder consolidation methods of spark plasma sintering (SPS) and hot pressing, respectively, under different thermal conditions. Since most HH compounds are synthesized by arc melting or induction melting, the significant difference in melting temperature of the involved constituents can lead to inhomogeneity and deviation of the matrix composition compared with nominal. This effect can be attributed to evaporation of low-melting-temperature phases or the difficulty in melting of higher-melting-temperature elements. Homogenization of the samples can be achieved by thermal treatments, which usually influence the microstructure and consequently the TE transport properties. Therefore, to understand the governing mechanisms and optimize the TE transport properties of HH compounds, these properties should be correlated to the specific apparent microstructure of the samples. In the class of HH compounds, the TE properties have so far been correlated to the apparent microstructure and the physical metallurgy conditions only for several compounds (e.g., ZrNiSn[12] and $Hf_{1-x}Zr_xNiSn_{1-y}Sb_y$[13]). In the current study, the microstructural evolution, following various heat treatments, of the *n*-type $Ti_{0.3}Zr_{0.35}Hf_{0.35}NiSn$ HH compound was correlated to the apparent TE transport properties, in an attempt to identify the governing microstructural mechanisms influencing the TE properties and to optimize the processing conditions of such samples.

EXPERIMENTAL PROCEDURES

Samples with the stoichiometric composition of $Ti_{0.3}Zr_{0.35}Hf_{0.35}NiSn$ were synthesized by arc melting

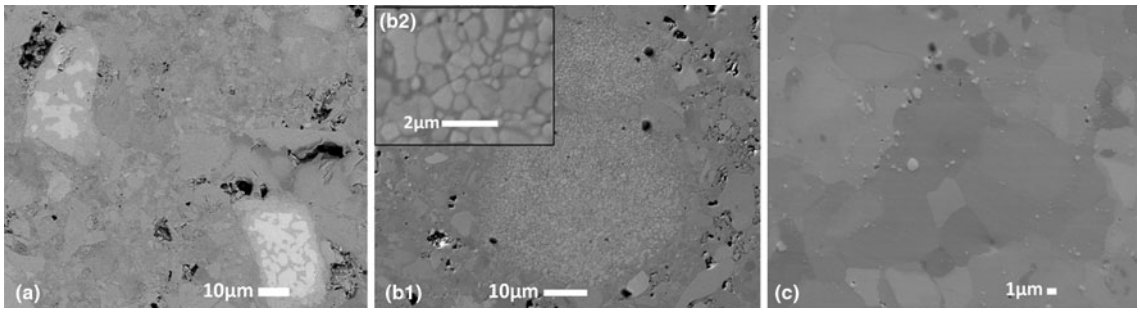

Fig. 2. SEM/back-scattered electron (BSE) micrographs of $Ti_{0.3}Zr_{0.35}Hf_{0.35}NiSn$ following SPS (a) and subsequent thermal treatments at 1163 K for 480 h (b) and 610 h (c).

of the pure (99.999%) metals Ti, Zr, Hf, Ni, and Sn under argon atmosphere. In the course of the arc melting, the samples were remelted and turned over three times. The synthesized ingots were milled for 5 h in a high-energy ball milling station (PM-100; Retsch, Germany) under a protective argon atmosphere. The powder had been filtered through a 60-mesh sieve and spark plasma sintered (SPS type HP D 5/1 FCT System GmbH, Germany) at 1373 K for 20 min (heating/cooling rates of 50 K/min) under mechanical pressure of 44 MPa and argon atmosphere of 4 Pa. Nearly fully dense (>99%) samples were obtained following SPS. Homogenization treatments under argon atmosphere were performed at 1163 K for 480 h and 610 h. All of the samples were characterized by x-ray powder diffraction. The x-ray data were collected on a Rigaku DMAX 2100 powder diffractometer with a graphite monochromator on the diffracted beam providing by Cu K_α radiation and operating at V = 40 kV, I = 30 mA. Scanning electron microscopy (SEM, JEOL JSM-5600; HRSEM, JEOL JSM-7400) was employed for microstructural characterizations. Seebeck coefficient and electrical resistivity values were measured in homemade equipment (measurement error 10%) under argon atmosphere up to 773 K. Electrical resistivity was measured by the four-probe method using an alternating power source of 1 V/50 Hz. An auxiliary heater was used to maintain a temperature difference of 10 K along the samples for Seebeck coefficient measurements. Thermal conductivity values were measured by the flash diffusivity method (LFA 457, NETZSCH) from room temperature to 773 K. The room-temperature carrier concentration of the samples was obtained by Hall-effect measurements using a self-constructed standard measurement apparatus at magnetic field of 0.8 T.

RESULTS AND DISCUSSION

The microstructures of the samples obtained following SPS and subsequent thermal treatments at 1163 K for 480 h and 610 h are shown in Fig. 2a, b, and c, respectively. Following the arc melting procedure, the samples exhibited large (10 μm to 20 μm), randomly scattered Hf-rich domains, which were still apparent following the SPS treatment (bright phase in Fig. 2a). The presence of these domains can be attributed to the high melting temperature of Hf (2504 K), which is higher than each of the other constituents, and the incomplete melting of this element in the course of the arc melting. Following thermal treatment at 1163 K for 480 h (Fig. 2b), decomposition of the large Hf-rich domains into smaller (1 μm to 2 μm) domains was observed, as shown in the inset, while additional thermal treatment at the same temperature for 610 h (Fig. 2c) decreased the domain size to the submicron range (<1 μm). Furthermore, following the 610 h thermal treatment, the density of the Hf-rich domains was dramatically reduced, an effect which can be attributed to the dissolution of these domains into the HH matrix, to approach the nominal composition of $Ti_{0.3}Zr_{0.35}Hf_{0.35}NiSn$. Nevertheless, even following this latter, prolonged heat treatment at 1163 K, complete elimination of these domains or complete homogenization of the HH phase was not reached.

Similar trends were also observed by XRD (Fig. 3). The diffraction patterns of as-received powder sample following SPS and additional thermal treatment are presented in Fig. 3a. On the same graph the 2θ positions of nominal solid solution are also marked by solid lines below. The lattice parameter of a nominal $Ti_{0.3}Zr_{0.35}Hf_{0.35}NiSn$ phase, 6.046 Å, was calculated assuming Vegard rule's for the three ordered HfNiSn, ZrNiSn, and TiNiSn HH phases with corresponding Pearson's lattice parameters of 6.084 Å, 6.10 Å, and 5.94 Å, respectively.

It can be observed from the figure that the peaks of the thermally treated samples are split in the vicinity of the nominal peaks, whereas the peaks of as-received powder sample are not split but are shifted relative to the nominal peaks towards small diffraction angle (clearly visible at higher 2θ angles). The estimated average lattice parameter for this phase was found to be a = 6.08 Å. The enlarged value of the average lattice parameter compared with the expected one can be attributed to the formation of disordered Heusler-based Cu_2MnAl phase, where the originally vacant sublattice is partially occupied. This disordering variant is

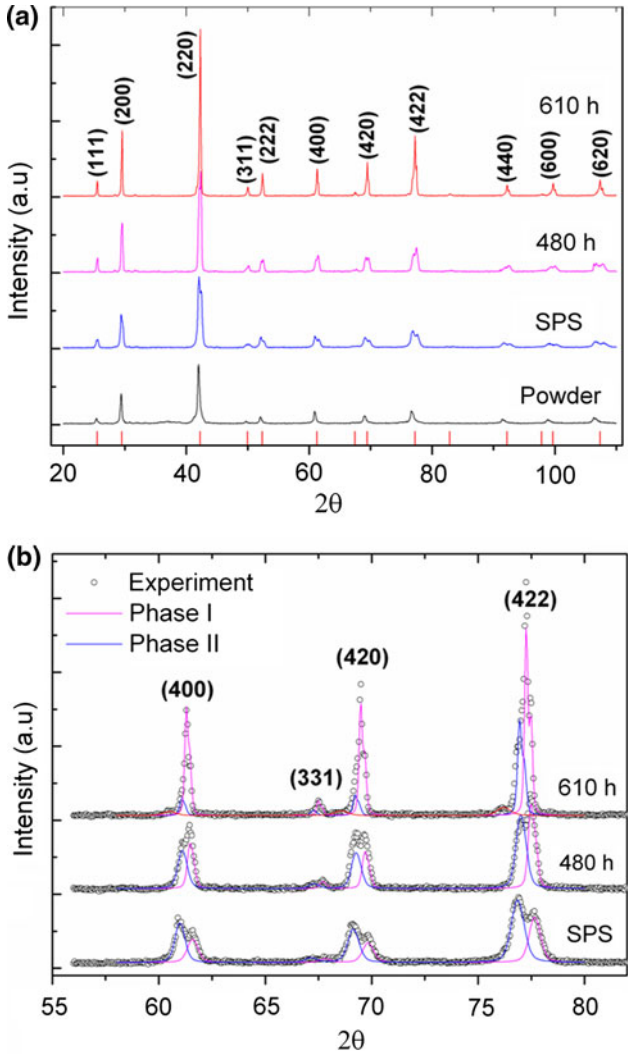

Fig. 3. Experimental (a) and Rietveld-fitted (b) XRD patterns of as-received $Ti_{0.3}Zr_{0.35}Hf_{0.35}NiSn$ powder, and following SPS and subsequent thermal treatments at 1163 K for 480 h and 610 h. The calculated 2θ positions for $Ti_{0.3}Zr_{0.35}Hf_{0.35}NiSn$ solution are marked by red lines.

consistent with the decrease of the (111)/(200) reflection intensities ratio, typically for the Cu_2MnAl structure.

The observed splitting of the x-ray peaks for the thermally treated samples indicates the formation of at least two solid solutions. Estimation of the 111/200/220 intensities ratio favors the ordered structure of MgAgAs type for each of the obtained HH phases rather than any disordered one. The lattice parameters and relative volume of the obtained phases were determined by analyzing the experimental XRD spectra by Rietveld procedure using PowderCell for Windows (PCW) software. A Rietveld plot of the calculated and experimental XRD spectra in the range $2\theta = 55°$ to $82°$ is shown in Fig. 3b.

The reflections are indexed in the setting of the cubic $F\bar{4}3m$ space group. The obtained lattice parameters and volume percent for all of the obtained phases are summarized in Table I.

Table I. Lattice parameters and volume percent for the obtained phases (Fig. 3b) following SPS and subsequent thermal treatments

Thermal Treatment	Phase I	Phase II
SPS	6.023 (40 vol.%)	6.076 (60 vol.%)
1163 K, 480 h	6.032 (47 vol.%)	6.065 (53 vol.%)
1163 K, 610 h	6.045 (80 vol.%)	6.060 (20 vol.%)

It can be seen from Table I that the thermal treatments tend to homogenize the apparent composition, in agreement with the microstructure observed following 1163 K/610 h thermal treatment (Fig. 2c).

The temperature dependencies of the TE properties, Seebeck coefficient, electrical resistivity, thermal conductivity, and the TE figure of merit, following SPS and subsequent thermal treatments at 1163 K for 480 h and 610 h, are shown in Figs. 4, 5, 6, and 7, respectively. From the negative and high Seebeck coefficient values obtained (Fig. 4), it is obvious that the samples are nearly TE-optimized *n*-type semiconductors. Complementary room-temperature carrier concentration values, measured using a Hall-effect apparatus, following SPS and 1163 K thermal treatment for 610 h, were found to be 8.67×10^{19} cm^{-3} and 4.00×10^{19} cm^{-3}, values which clearly indicate highly electronically optimized materials. Furthermore, the reduction of the carrier concentrations with increasing thermal treatment duration is in agreement with the general trends of increase of both Seebeck coefficient and electrical resistivity values. It is noteworthy that, although the Seebeck coefficient values for any given temperature, following the various thermal treatments, fall within the measurement error (~10%), the general temperature dependence trend following each of the above-mentioned thermal treatments is in agreement with both the carrier concentration and electrical resistivity trends. All these trends, indicating a reduction of the carrier concentration with increasing heat treatment duration, are in agreement with the microstructural and phases evolution shown in Figs. 2 and 3, respectively, and clearly imply reduction of the relative amount of the metallic Hf-rich phase.

The total thermal conductivity values, indicated in Fig. 6, were experimentally measured following SPS and theoretically estimated following the thermal treatments at 1163 K for 480 h and 610 h, by assuming constant lattice thermal conductivity, κ_l, values, obtained following SPS, and using electronic thermal conductivity, κ_e, values calculated by the Wiedemann–Franz relation ($\kappa_e = LT/\rho$, where L is the Lorenz number, being 2.45×10^{-8} W Ω/K^2 for

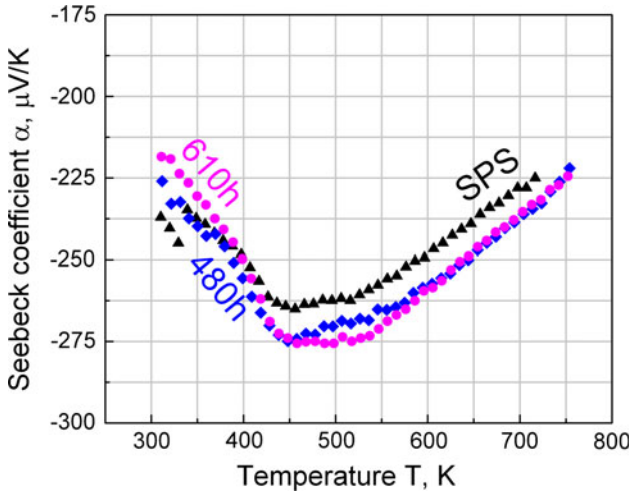

Fig. 4. Temperature dependence of the Seebeck coefficient of $Ti_{0.3}Zr_{0.35}Hf_{0.35}NiSn$ following SPS and subsequent thermal treatments at 1163 K for 480 h and 610 h.

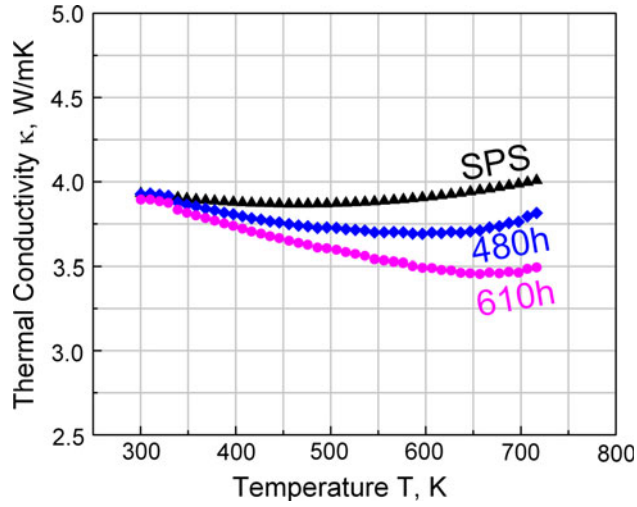

Fig. 6. Temperature dependence of the thermal conductivity of $Ti_{0.3}Zr_{0.35}Hf_{0.35}NiSn$ following SPS and subsequent thermal treatments at 1163 K for 480 h and 610 h.

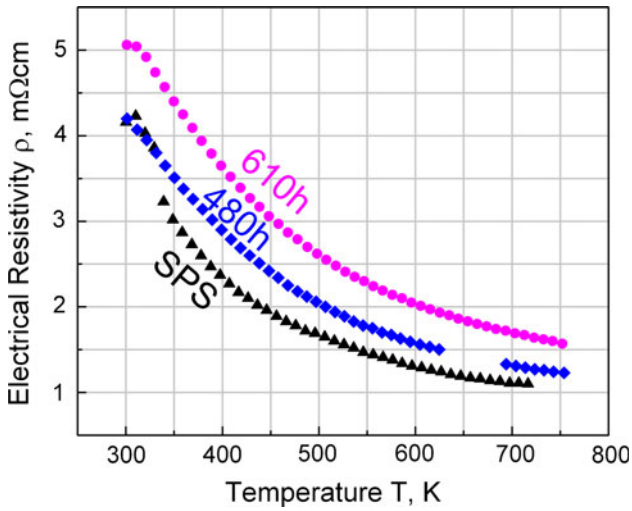

Fig. 5. Temperature dependence of the electrical resistivity of $Ti_{0.3}Zr_{0.35}Hf_{0.35}NiSn$ following SPS and subsequent thermal treatments at 1163 K for 480 h and 610 h.

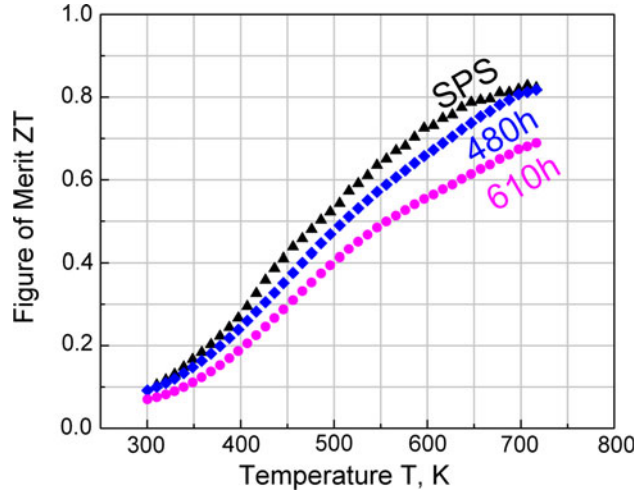

Fig. 7. Temperature dependence of the dimensionless thermoelectric figure of merit of $Ti_{0.3}Zr_{0.35}Hf_{0.35}NiSn$ following SPS and subsequent thermal treatments at 1163 K for 480 h and 610 h.

degenerated conditions, T is the absolute temperature, and ρ is the measured electrical resistivity value from Fig. 5). Although a size reduction trend of the Hf-rich domains down to the submicron range was observed with increasing thermal treatment duration (Fig. 2), an effect which can possibly result in reduction of the lattice thermal conductivity, constant κ_l values were taken into account for estimation of the total thermal conductivities following the 1163 K thermal treatment to provide a lower bound for ZT estimation.

From the ZT values following the various heat treatments (Fig. 7), it can be seen that very high ZT values of up to ~0.82 were obtained following SPS, clearly indicating the high TE potential of the investigated composition. These ZT values were slightly reduced, down to $ZT_{max} \approx 0.7$, following the subsequent thermal treatments. However, it should be taken into account that these ZT values are lower bounds, as theoretically estimated, taking into account no lattice thermal conductivity variations following SPS. Consequently, there is no doubt that the investigated composition exhibits maximal ZT values of at least 0.7 up to the maximal investigated temperature of ~730 K, which was limited by our available characterization apparatus. The obtained ZT values are higher than previously reported values for $Ti_xZr_yHf_{1-x-y}NiSn$ compounds with similar

nominal compositions (curves e and g in Fig. 1),[14,15] obtained by different preparation techniques.

CONCLUSIONS

The evolution of the microstructural and TE properties of the *n*-type $Ti_{0.3}Zr_{0.35}Hf_{0.35}NiSn$ HH compound following SPS and subsequent thermal treatments at 1163 K for 480 h and 610 h were investigated and correlated. Nearly optimized TE values were obtained following the investigated conditions, showing high maximal *ZT* values in the range of 0.7 to 0.82 at ~730 K. The evolution of the TE properties, influenced by a reduction of the carrier concentration in the course of the thermal treatment, was attributed to the dissolution of high-melting-temperature metallic Hf-rich domains, which were originally apparent following arc melting. This latter result clearly demonstrates the sensitivity of the microstructure and consequently the TE properties of the investigated system to the employed preparation techniques. The presented approach was found to be very useful for understanding the microstructural effects of the complicated HH phases on the TE properties and for clarifying the discrepancy between previously reported values of TE properties for similar HH compositions obtained using different preparation conditions.

REFERENCES

1. Y. Gelbstein, N. Tal, A. Yarmek, Y. Rosenberg, M.P. Dariel, S. Ouardi, B. Balke, C. Felser, and M. Köhne, *J. Mater. Res.* 1, 1 (2011).
2. H.J. Goldsmid, *Applications of Thermoelectricity* (New York: Wiley, 1960).
3. F. Casper, T. Graf, S. Chadov, B. Balke, and C. Felser, *Semicond. Sci. Technol.* 27, 063001 (2012).
4. W. Jeitschko, *Metall. Mater. Trans. B* 1, 3159 (1970).
5. F. Aliev, N. Brandt, V. Moshchalkov, V. Kozyrkov, R. Skolozdra, and A. Belogorokhov, *Zeitschrift für Physik B Condens. Matter.* 75, 167 (1989).
6. T. Graf, C. Felser, and S.S.P. Parkin, *Prog. Solid State Chem.* 39, 1 (2011).
7. J. Callaway and H.C. von Baeye, *Phys. Rev.* 120, 1149 (1960).
8. C. Uher, J. Yang, S. Hu, D. Morelli, and G. Meisner, *Phys. Rev. B.* 59, 8615 (1999).
9. H. Hohl, A.P. Ramirez, C. Goldmann, G. Ernst, B. Wölfing, and E. Bucher, *J. Phys.: Condens. Matter* 11, 1697 (1999).
10. S.R. Culp, S.J. Poon, N. Hickman, T.M. Tritt, and J. Blumm, *Appl. Phys. Lett.* 88, 042106 (2006).
11. N. Shutoh and S. Sakurada, *J. Alloys Compd.* 389, 204 (2005).
12. H. Xie, J. Mi, L. Hu, N. Lock, M. Chirstensen, C. Fu, B.B. Iversen, X. Zhao, and T. Zhu, *CrystEngComm* 14, 4467 (2012).
13. C. Yu, T. Zhu, R. Shi, Y. Zhang, X. Zhao, and J. He, *Acta Mater.* 57, 2757 (2009).
14. K. Kurosaki, H. Muta, and S. Yamanaka, *J. Alloys Compd.* 384, 51 (2004).
15. K. Kurosaki, T. Maekawa, H. Muta, and S. Yamanaka, *J. Alloys Compd.* 397, 296 (2005).
16. M. Tang and J. Zhao, *J. Alloys Compd.* 475, 5 (2009).
17. S. Populoh, M. Aguirre, O. Brunko, K. Galazka, Y. Lu, and A. Weidenkaff, *Scr. Mater.* 66, 1073 (2012).